

## Macrophage-Derived IL1 $\beta$ and TNF $\alpha$ Regulate Arginine Metabolism in Neuroblastoma

Livingstone Fultang<sup>1</sup>, Laura D. Gamble<sup>2</sup>, Luciana Gneo<sup>1</sup>, Andrea M. Berry<sup>3</sup>, Sharon A. Egan<sup>4</sup>, Fenna De Bie<sup>1</sup>, Orli Yogev<sup>5</sup>, Georgina L. Eden<sup>2</sup>, Sarah Booth<sup>1</sup>, Samantha Brownhill<sup>3</sup>, Ashley Vardon<sup>1</sup>, Carmel M. McConville<sup>6</sup>, Paul N. Cheng<sup>7</sup>, Murray D. Norris<sup>2</sup>, Heather C. Etchevers<sup>8</sup>, Jayne Murray<sup>2</sup>, David S. Ziegler<sup>2</sup>, Louis Chesler<sup>5</sup>, Ronny Schmidt<sup>9</sup>, Susan A. Burchill<sup>3</sup>, Michelle Haber<sup>2</sup>, Carmela De Santo<sup>1</sup>, and Francis Mussai<sup>1</sup>



### Abstract

Neuroblastoma is the most common childhood solid tumor, yet the prognosis for high-risk disease remains poor. We demonstrate here that arginase 2 (ARG2) drives neuroblastoma cell proliferation via regulation of arginine metabolism. Targeting arginine metabolism, either by blocking cationic amino acid transporter 1 (CAT-1)-dependent arginine uptake *in vitro* or therapeutic depletion of arginine by pegylated recombinant arginase BCT-100, significantly delayed tumor development and prolonged murine survival. Tumor cells polarized infiltrating monocytes to an M1-macrophage phenotype, which released IL1 $\beta$  and TNF $\alpha$  in a RAC-alpha serine/threonine-protein kinase (AKT)-dependent manner. IL1 $\beta$  and TNF $\alpha$  established a

feedback loop to upregulate ARG2 expression via p38 and extracellular regulated kinases 1/2 (ERK1/2) signaling in neuroblastoma and neural crest-derived cells. Proteomic analysis revealed that enrichment of IL1 $\beta$  and TNF $\alpha$  in stage IV human tumor microenvironments was associated with a worse prognosis. These data thus describe an immune-metabolic regulatory loop between tumor cells and infiltrating myeloid cells regulating ARG2, which can be clinically exploited.

**Significance:** These findings illustrate that cross-talk between myeloid cells and tumor cells creates a metabolic regulatory loop that promotes neuroblastoma progression.

### Introduction

The consumption and metabolism of diverse nutrients by cancer cells is recognized as a key regulator of immunity. Glucose metabolism by cancer cells generates a tumor microenvironment that has low levels of glucose, leading to inhibition of T-cell cytotoxicity through the accumulation of lactate, microenvironment acidification, and reduced aerobic glycolysis (1–3). Tumor-infiltrating monocyte differentiation and cytokine release may be similarly affected, leading to perturbation of their role in coordinating the surrounding immune response (4, 5). Amino acid

metabolism also plays a critical role in the function of both normal and malignant cells. Although whole body amino acid homeostasis is regulated through restricted interorgan enzyme expression, at the cellular level, enzyme expression is controlled in the intracellular compartment to maintain metabolic precursor supplies and regulate the wider tissue microenvironment (6).

Arginine is a semiessential amino acid that is metabolized into ornithine and urea by the expression of cytoplasmic arginase 1 (ARG1) and mitochondrial arginase 2 (ARG2), or nitric oxide synthase enzymes into reactive nitric oxide species (7). These metabolites feed forward into diverse roles in cell signaling, proliferation, and protein synthesis. Cellular breakdown of arginine also plays a critical role in regulating the immune response, a process that has been capitalized on by malignant cells to contribute to their immune escape (8). We recently identified that acute myeloid leukemias (AML) and neuroblastoma, two of the most common and devastating cancers of childhood, create a potent immunosuppressive microenvironment through the expression of the ARG2 enzyme, which suppresses T-cell immunity (9, 10).

Although the metabolic effect of cancer cells on shaping the responsiveness of surrounding immune populations is increasingly well described, the reciprocal effects of immune cell populations on modulating cancer cell amino acid metabolism have not previously been reported. In particular, the role of arginine metabolism in this process is unknown, and the signals that regulate ARG2 in cancer are not well understood. Here we demonstrate how myeloid cells within the tumor microenvironment and tumor cells engage in reciprocal cross-talk to regulate the

<sup>1</sup>Institute of Immunology and Immunotherapy, University of Birmingham, Birmingham, UK. <sup>2</sup>Children's Cancer Institute, University of New South Wales, Sydney, Australia. <sup>3</sup>Children's Cancer Research Group, Leeds Institute of Cancer and Pathology, University of Leeds, Leeds, UK. <sup>4</sup>School of Veterinary Medicine and Science, Sutton Bonington Campus, University of Nottingham, Nottingham, UK. <sup>5</sup>The Institute of Cancer Research, London, UK. <sup>6</sup>Institute of Cancer Genomic Sciences, University of Birmingham, Birmingham, Birmingham, UK. <sup>7</sup>Bio-Cancer Treatment International, Hong Kong. <sup>8</sup>GMGF, Aix Marseille University, INSERM, Marseille, France. <sup>9</sup>Sciomics GmbH, Heidelberg, Germany.

**Note:** Supplementary data for this article are available at Cancer Research Online (<http://cancerres.aacrjournals.org/>).

C. De Santo and F. Mussai contributed equally to this article.

**Corresponding Author:** Francis Mussai, Institute of Immunology and Immunotherapy, University of Birmingham, Birmingham B15 2TT, UK. Phone: 44-121-414-7047; E-mail: francis.mussai@nhs.net

**doi:** 10.1158/0008-5472.CAN-18-2139

©2018 American Association for Cancer Research.

Fultang et al.

expression of ARG2 in neuroblastoma cells, and how this arginine metabolism plays a central role in neuroblastoma pathogenesis. Importantly, this study identifies arginine metabolism as a clinically relevant therapeutic target.

## Materials and Methods

### Patient samples

Heparinized blood and tumor samples were obtained from 50 patients with neuroblastoma treated at the Birmingham Children's Hospital and Children's Hospital Oxford. Samples were obtained from patients with newly diagnosed neuroblastoma, at the time of diagnostic biopsy or before the start of treatment. GD2<sup>+</sup> neuroblastoma cells were isolated from bone marrow aspirates taken from patients with stage IV disease.

### Neuroblastoma murine model

Transgenic Tg(*TH-MYCN*)<sup>41Waw</sup> mice were genotyped to detect the presence of human *MYCN* transgene or the chromosome 18 insertion site, using an allelic discrimination methodology (11, 12). Specific assays were designed to measure the presence of the *MYCN* transgene (forward primer 5'-CGACCACAAGGCCCT-CAGTA; reverse primer 5'-CAGCCTTGTTGGAGGAG; probe 6FAM-CGCTTCTCCACAGTGACCACGTCG TAMRA; Eurofins) or to the site of the transgene on chromosome 18, which is disrupted during insertion (forward primer 5'-CCACAAAATATGACTTCC-TAAAAGATT; reverse primer 5'-CATGGGACTTCCCTTATATGCT; probe VIC-5'-AACAAATTATAACACCATTAGATATG TAMRA). After weaning, *TH-MYCN* mice were palpated for intra-abdominal tumors twice weekly. Mice with palpable tumors ranging in size between 5 and 20 mm in diameter were then humanely sacrificed. At sacrifice, unheparinized and heparinized whole blood, as well as tumor tissue were obtained for further *ex vivo* analyses. Tumor tissue was processed as above. Tumor tissues were stained with anti-mouse GD2 (BioLegend) on ice for 30 minutes. The expression of these markers was then assessed by flow cytometry.

For treatment with BCT-100, mice were treated with 60 mg/kg BCT-100 or saline, twice a week, *i.p.*, either from weaning in the prophylaxis setting or upon the development of a 5-mm tumor in the treatment setting. Mice were treated until the experimental endpoint of a 10-mm abdominal tumor. In the prophylaxis experiment, mice were bled before the start of treatment, midway through the treatment, 24 hours after the fifth dose of either saline or BCT-100, and at tumor endpoint. All experimental protocols were monitored and approved by either The Institute of Cancer Research Animal Welfare and Ethical Review Body, in compliance with guidelines specified by the UK Home Office Animals (Scientific Procedures) Act 1986, and the United Kingdom National Cancer Research Institute guidelines for the welfare of animals in cancer research or the University of New South Wales Animal Care and Ethics Committee and conducted according to the Animal Research Act, 1985 (New South Wales, Australia), and the Australian Code of Practice for Care and Use of Animals for Scientific Purposes (2013).

### GD2<sup>+</sup> tumor cell and myeloid cell isolation

For isolation of GD2<sup>+</sup> tumor cells from human and murine tumors were digested using type II collagenase, labeled with anti-GD2-PE antibody (BioLegend), and bound to anti-PE-coated magnetic beads (Miltenyi Biotec). Cells were enriched according

to the manufacturer's instructions to be >98% GD2<sup>+</sup> cells as confirmed by flow cytometry using a PE-conjugated anti-human GD2 antibody. For isolation of primary GD2<sup>+</sup> cells from the bone marrow of diagnosed stage IV patients, bone marrow aspirates were collected in RPMI 1640 media containing 10% FCS. Cells were lysed using erythrocyte lysis buffer (Qiagen) and the white cell fraction isolated by centrifugation. Neuroblastoma cells were labeled with purified mouse anti-human GD2 Clone 14.G2a (BD Pharmingen) and bound to anti-mouse IgG2a/b microbeads (Miltenyi Biotec). Cells were enriched according to the manufacturer's instructions (Miltenyi Biotec). For isolation of monocytes, peripheral blood was collected from healthy donors. Monocytes were separated using a Lymphoprep gradient (STEMCELL Technologies) and enriched by positive selection using anti-human CD14 MicroBeads (Miltenyi Biotec).

### Cell lines and cultures

Human primary, untransformed, embryonic neural crest (R1113T) or dorsal root and/or sympathetic ganglion-derived stem cells (SZ16) were obtained and cultured as previously described (13–15). Neuroblastoma cell lines (SKNAS, KELLY, IMR-32, and LAN-1), the Ewing sarcoma cell line SKNMC, which has high ARG2 expression, and primary GD2<sup>+</sup> neuroblastoma cells were cultured in RPMI 1640 medium (Sigma) supplemented with 10% *v/v* fetal bovine serum (FBS, Sigma), 100 U/mL penicillin and streptomycin (Gibco), 1 mmol/L sodium pyruvate (Gibco), and 2 mmol/L *L*-glutamine (Gibco). All cell lines were originally obtained from ATCC and validated for authenticity by DNA short tandem repeats in line with American National Standards Institute ASN-0002-2011 (Northgene). All experiments were performed between passages 3 and 9, and cells were confirmed as *Mycoplasma* negative by PCR analysis (LookOut, SIGMA; latest testing date September 2018). The effects of arginine deprivation were tested on cells cultured in arginine-free RPMI 1640 for SILAC (Thermo Fisher Scientific) supplemented with 10% *v/v* arginine-free dialyzed FBS (Thermo Fisher Scientific). Cells were maintained in an incubator at 5% CO<sub>2</sub> in air and at 37°C.

### Arginase activity assays

The activity of arginase 2 present within cells was determined by measuring the conversion of arginine into urea, as previously described (10).

### Antibody microarray analysis

Human stage I neuroblastoma tissue samples ( $n = 13$ ) and human stage IV neuroblastoma biopsies ( $n = 9$ ) were analyzed using scioDiscover antibody microarrays (Sciomics), which target 900 cancer-related proteins (16). After sample homogenization, proteins were extracted with scioExtract buffer (Sciomics) and labeled at an adjusted concentration with scioDye 2 (Sciomics) according to the manufacturer's instructions. A pool of all protein samples was labeled with scioDye1 and used as a reference for all experiments, allowing competitive dual-color measurements. Array production, blocking, and sample incubation were performed in compliance with strict quality control procedures as reported previously. The arrays were scanned with identical instrument laser power and adjusted PMT setting using a Power-scanner (Tecan). Spot segmentation was performed with the software GenePix Pro 6.0 (Molecular Devices).

## ELISA

The concentrations of cytokines IFN $\gamma$ , IL1 $\beta$ , TNF $\alpha$ , TGF $\beta$ , IL6, IL4, IL13, and GM-CSF in plasma and cell culture media were measured by the sandwich-ELISA kit according to specific manufacturer's instructions.

## Monocyte-driven proliferation assays

Neuroblastoma cells suspended at a density of  $1 \times 10^6$  cells/mL in PBS were labeled with 1  $\mu$ mol/L CellTrace FarRed staining solution (Molecular Probes, Thermo Fisher Scientific) at 37°C for 20 minutes. Stained cells were washed three times in RPMI-1640 and rested for 10 minutes in complete media. Labeled neuroblastoma cells were then cultured in supernatants from neuroblastoma-induced macrophages (75% final volume), with or without 1  $\mu$ g/mL anti-IL1 $\beta$  (R&D Systems, catalog #MAB201) and 1 ng/mL anti-TNF $\alpha$  (Cell Signaling, catalog #7321s) neutralizing antibodies. Cells were harvested 5 days later and analyzed on a CytoFLEX Flow Cytometer (Beckman Coulter). Histograms representing distinct generations of proliferation cells were generated using the FlowJo Software (TreeStar Inc.).

## Reverse transcriptase PCRs

Total RNA was extracted from cells using either the RNEasy Kit (Qiagen) according to the manufacturer's specifications. Extracted RNA was quantified on a NanoDrop ND-1000 spectrophotometer (Thermo Scientific). First-strand complementary DNA (cDNA) was generated by incubating 1  $\mu$ g of extracted RNA with 500 ng of random primers (Promega), 0.5 mmol/L dNTP (Promega), 1 $\times$  reverse transcriptase buffer (Promega), 40U RNase inhibitors (RNasin, Promega) and either 100U MMLV RNase H+ or 15U AMV reverse transcriptase (Promega). For endpoint PCR reactions, up to 100 ng of sample cDNA was incubated in 5  $\mu$ L of 10 $\times$  PCR reaction buffer (Invitrogen), 0.5 mmol/L dNTPs, one unit of Taq polymerase (Invitrogen), 1.5 mmol/L MgCl $_2$ , 0.5  $\mu$ mol/L of each forward and reverse primer and nuclease free water up to a final reaction volume of 50  $\mu$ L. Human primer sequences are listed in Supplementary Table S1. All quantitative PCR (RT-qPCR) reactions were conducted on a Fast 7500 real-time PCR thermal cycler (Applied Biosystems).

## TaqMan assays

RNA was isolated using the miRNeasy Mini Kit (Qiagen), and RNA concentration determined by spectrophotometry (NanoDrop 1000, Thermo Fisher Scientific). RNA (10 ng per replicate) was reverse transcribed using Superscript III Reverse Transcriptase (Thermo Fisher Scientific) according to the manufacturer's instructions with random hexamer primers (0.3  $\mu$ g, Thermo Fisher Scientific) and RNasin Plus RNase Inhibitor (20 units, Promega). Samples were analyzed in triplicate. Samples analyzed in the absence of RT enzyme or without RNA were included as negative controls. cDNA was amplified using TaqMan Gene-Expression Assays for each target (Supplementary Table S1; Thermo Fisher Scientific) according to the manufacturer's instructions. Expression of the housekeeping gene PPIA was determined for each sample using sequence-specific reverse and forward primers (200 nmol/L forward primer GGACCAACA-CAAATGGTTC, 200 nmol/L reverse primer CTTTCACTTGC-CAAACACCA, 100 nmol/L FAM-labeled probe ATGCTTGC-CATCCAACCACTCAGTCTTG). mRNA expression was calculated using the comparative Ct method relative to PPIA. RNA from cell

lines known to express genes of interest were included as control (Supplementary Table S1).

## Study approval

In accordance with the Declaration of Helsinki, patient samples were obtained after written informed consent prior to inclusion in the study. Primary human neural crest-derived stem cell lines were obtained under ethical committee approval PFS14-011 from the French Biomedical Agency for the use of embryonic material. Regional ethics committee (REC 10/H0501/39) and local hospital trust research approval for the study was granted for UK hospitals. The Institute of Cancer Research Ethics Committee approved all animal protocols in this study. Collection of diagnostic bone marrow aspirates from stage IV patients was performed under ethical approval of the Medical Research and Ethics committee (MREC/98/4/023). Procedures were carried out in accordance with UK Home Office Guidelines.

## Antibody microarray normalization and statistical analysis

The acquired raw data were analyzed using the linear models for microarray data (LIMMA) package of R-Bioconductor after uploading the median signal intensities. As described previously, a specialized invariant Lowess method was applied for normalization (17). For the differential analysis of protein expression, a one-factorial linear model was fitted with LIMMA, resulting in a two-sided *t* test or *F* test based on moderated statistics. Differences in protein abundance between sample groups are presented as log-fold changes (logFC) calculated for the basis 2. The presented *P* values were adjusted for multiple testing by controlling the false discovery rate according to Benjamini and Hochberg. In all comparisons, proteins were defined as significantly differential with a logFC above 0.5 or below -0.5 and an adjusted *P* value below 0.05. Functional enrichment analyses were conducted with the STRING software (<https://string-db.org>) for the proteins with significantly differential abundance between groups, whereby upregulated and downregulated proteins were analyzed separately.

## Arginase 2 fluorescence intensity

Quantification of cell-by-cell fluorescence intensity for arginase 2 expression across treatment conditions were performed using ImageJ software (NIH). Briefly, confocal image stacks were converted to single channel images. Pixel intensity measurements were determined from single channel images representing arginase 2 staining with image thresholds set to match positive structures within defined cell boundaries.

## Statistical analysis

Parametric Student *t* tests were used to determine the statistical significance of the difference in paired observations between groups (GraphPad Prism). All *P* values are two-tailed, and *P* values <0.05 were considered to represent statistically significant events. Significance was recorded as \*, *P* < 0.05; \*\*, *P* < 0.01; \*\*\*, *P* < 0.001; \*\*\*\*, *P* < 0.0001.

## Results

### Neuroblastoma-conditioned macrophages release IL1 $\beta$ and TNF $\alpha$ in the tumor microenvironment

Myeloid cells are a major orchestrator of cancer-related inflammation with the potential to support tumor growth, invasion, and

metastasis. In neuroblastoma, we have previously shown a significant increase of immunosuppressive myeloid cells in the peripheral blood of patients and in the tumor tissue of the transgenic neuroblastoma TH-MYCN murine model. However, the role of intratumoral myeloid cells in human neuroblastoma tumors is not well understood. To understand the landscape inside human tissue at diagnosis, we first investigated the proteomic profile of 23 human neuroblastoma tumors (9 stage I and 14 stage IV) using a novel antibody array (18). Nonmetric multidimensional scaling from protein array for all analyzed samples based on the complete protein expression data revealed separate clustering of stage I and IV tumors (Fig. 1A). Analysis of human neuroblastoma proteomes showed increased expression of the monocyte/macrophage marker CD14 and the granulocytic cell marker CD15 in high-stage disease (Fig. 1B). IHC of tissue microarrays of 27 tumors revealed that CD14<sup>+</sup> cells infiltrated the tumor tissue (Fig. 1C, top plots with histoscore, Fig. 1D; Supplementary Fig. S1A), while CD15 staining localized around vasculature (Fig. 1C, bottom plots with histoscore, Fig. 1D; Supplementary Fig. S1A). Together, these findings highlight the potential role of myeloid cells in tumorigenesis.

Monocyte function may be modulated by their environment. To investigate the influence of neuroblastoma tumor cells on monocytes, monocytes enriched from healthy donor blood were cocultured with sorted Ganglioside G2 (GD2)<sup>+</sup> neuroblastoma cells from patients or cell lines. We observed that neuroblastoma conditioning led to upregulation of the macrophage marker CD68 and only a minority of cells upregulated CD206 (M2 marker; Fig. 1E; Supplementary Fig. S1B and S1C). In addition, myeloid ARG1 activity was downregulated (Fig. 1F), consistent with polarization to an M1 phenotype. Importantly, IHC of neuroblastomas at diagnosis confirmed the infiltration of these CD68<sup>+</sup> macrophages within the tumor tissue (Fig. 1G; Supplementary Fig. S1D).

Tumor-infiltrating myeloid cells can shape the immune response through cytokine release within tumor tissue (19). To investigate the cytokine profile of neuroblastoma-induced macrophages, a broad panel of cytokines was analyzed in culture supernatants. Tumor-conditioning led to an increased release of IL1 $\beta$  and TNF $\alpha$ , with undetectable levels of IL13, IL6, IFN $\gamma$ , IL4, TGF $\beta$ , and GM-CSF consistent with an M1 phenotype (Fig. 2A and B; Supplementary Fig. S2A). Tumor cells alone released minimal cytokines (<8 pg/mL; Supplementary Fig. S2B). Although CD15<sup>+</sup> granulocytes released IL8, they did not release either IL1 $\beta$  or TNF $\alpha$  following tumor coculture (Supplementary Fig. S2C). To prove that the release of IL1 $\beta$  and TNF $\alpha$  was from the macrophages, intracellular staining for cytokines was performed. Neuroblastoma conditioning led to an increased frequency of IL1 $\beta$  and TNF $\alpha$ -positive macrophages at 24 and 48 hours (Fig. 2C; Supplementary Fig. S3A and S3B). Using confocal microscopy, we confirmed CD14<sup>+</sup> cells sorted from patients expressed IL1 $\beta$  and TNF $\alpha$  (Supplementary Fig. S3C) and IHC of tissue microarrays of 27 tumors confirmed the expression of IL1 $\beta$  and TNF $\alpha$  in the tumor-infiltrating macrophages (Fig. 2D; Supplementary Fig. S4A).

IL1 $\beta$  and TNF $\alpha$  secretion from myeloid cells may be regulated by AKT signaling (20). Coculture of healthy donor monocytes with neuroblastoma led to AKT phosphorylation (Fig. 2E) and AKT inhibition with MK-2206 prevented IL1 $\beta$  and TNF $\alpha$  release (Fig. 2F and G). No evidence for STAT3, NF- $\kappa$ B, or PI3K pathway activation was identified (Supplementary Fig. S4B). Therefore,

neuroblastoma cells polarize surrounding monocytes to M1 macrophages that release IL1 $\beta$  and TNF $\alpha$ .

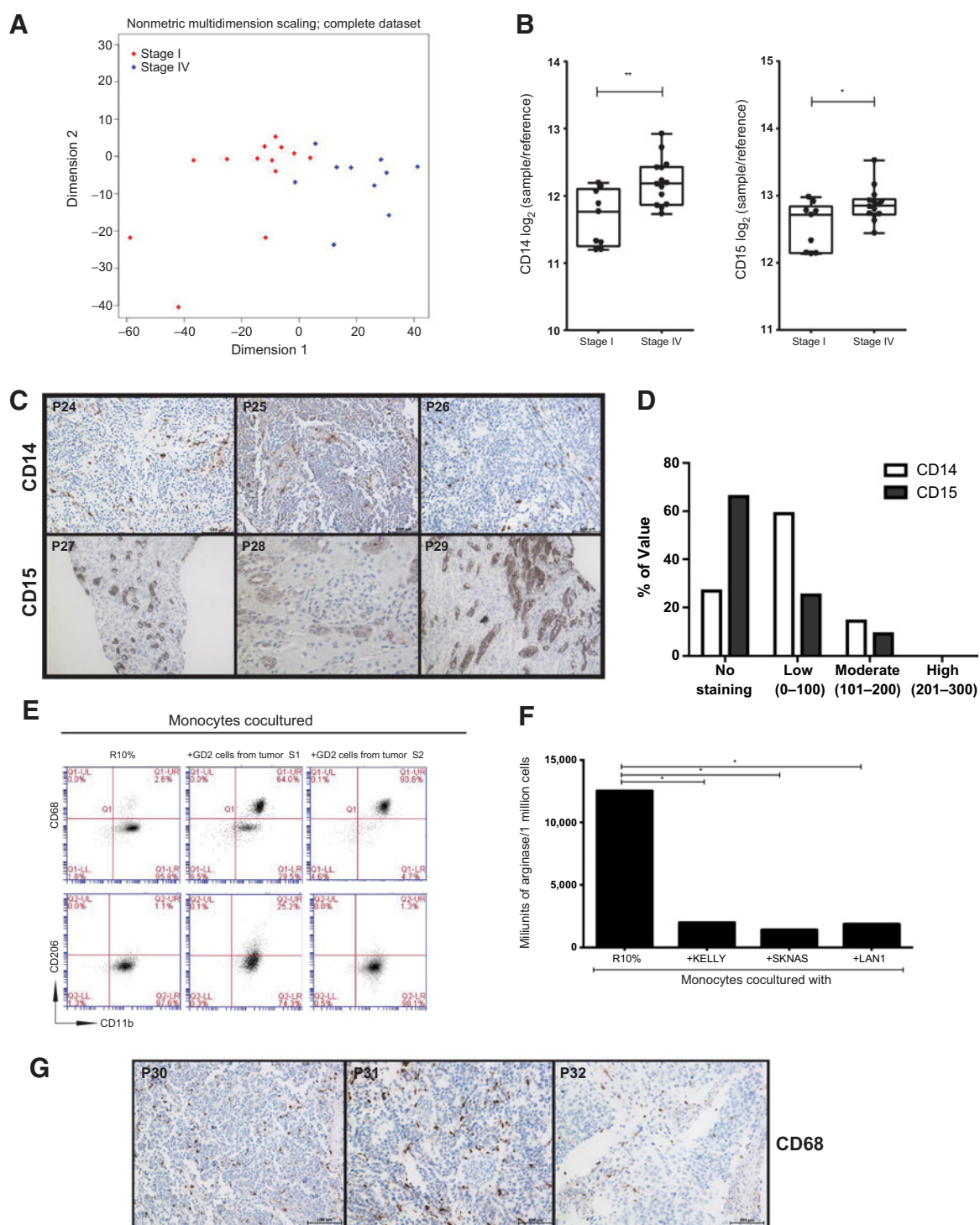
### Neuroblastoma cell proliferation is dependent on arginine metabolism

Previously, we established that neuroblastoma cells consume arginine from the microenvironment and catabolize this amino acid by ARG2 to create an immunosuppressive microenvironment contributing to immune escape and suboptimal immunotherapy responses (9). However, the role of ARG2 in neuroblastoma development and more widely in human cancers has received only limited study. Arginine metabolism can contribute to cell proliferation. To investigate the role of ARG2 in tumor cell proliferation, we first performed shRNA knockdown for ARG2. ARG2 knockdown led to a significant reduction in cell proliferation (Fig. 3A; Supplementary Fig. S4C), confirming the key role of this enzyme. We next blocked the uptake of arginine from the microenvironment via cationic amino acid transporter-1 (CAT1), which we showed is expressed in the majority of neuroblastoma cell lines (Supplementary Fig. S4D). N-nitro-L-arginine (L-NAME) inhibitor led to a significant decrease in tumor cell proliferation (Fig. 3B). Culture of tumor cells in the absence of arginine similarly inhibited tumor cell metabolic activity (Fig. 3C). BCT-100 is a PEGylated recombinant human arginase that can deplete arginine to undetectable levels in patients with cancer, leading to clinical responses in adult trials (21). Culture of neuroblastoma with BCT-100 led to a rapid inhibition of cell proliferation (Supplementary Fig. S4E), and tumor cell death characterized by PARP cleavage (Supplementary Fig. S5A). Electron microscopy of sorted tumor cells from cell lines and patients confirms loss of cell membrane integrity and cellular fragmentation (Fig. 3D).

To investigate the *in vivo* dependence of tumor growth on arginine, we used the immunocompetent TH-MYCN transgenic mouse model, which spontaneously developed neuroblastoma tumors (11). These murine tumor cells also express ARG2 (Supplementary Fig. S5B). We first demonstrated that *ex vivo* treatment of murine GD2<sup>+</sup> tumor cells with BCT-100 led to a significant reduction in viable cells (Fig. 3E). Treatment of TH-MYCN mice with twice-weekly BCT-100 led to a sustained drop in plasma arginine to almost undetectable levels (Fig. 3F). To understand if tumor initiation could be delayed or prevented in the absence of arginine, mice were treated prophylactically from the time of weaning at 3 weeks of age, when the tumors were 1 to 2 mm in size. Neuroblastoma development was significantly delayed, and mice survived for significantly longer in the BCT-100-treated group compared with control ( $P = 0.0001$ ; Fig. 3G). Following this, we investigated the effect of BCT-100 on established tumors. Here we showed that murine tumor progression was significantly delayed compared with the saline control, and overall survival was significantly extended ( $P = 0.0181$ ; Fig. 3H). Arginine resynthesis pathway enzymes argininosuccinate synthase and ornithine transcarbamylase (OTC) were not upregulated in GD2<sup>+</sup> cells from murine tumors as mechanisms of resistance (Supplementary Fig. S5C). No evidence for BCT-100 drug toxicity in terms of weight or clinical features were identified.

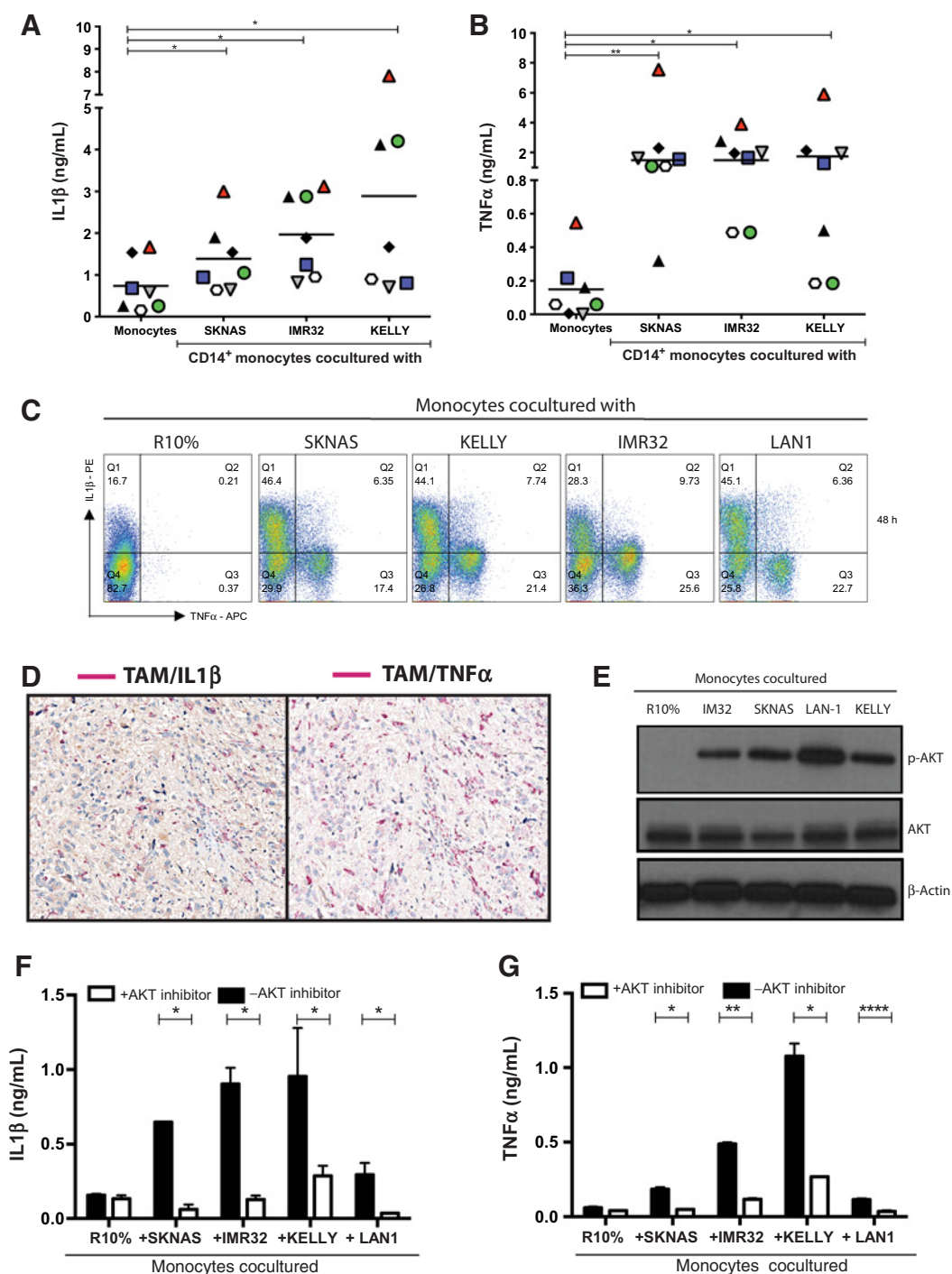
### Macrophage IL1 $\beta$ and TNF $\alpha$ drive tumor ARG2 expression via p38/ERK signaling

As ARG2 contributes to tumor cell proliferation, we hypothesized that these macrophage-derived cytokines may reciprocally regulate ARG2 expression. We first showed that the treatment of

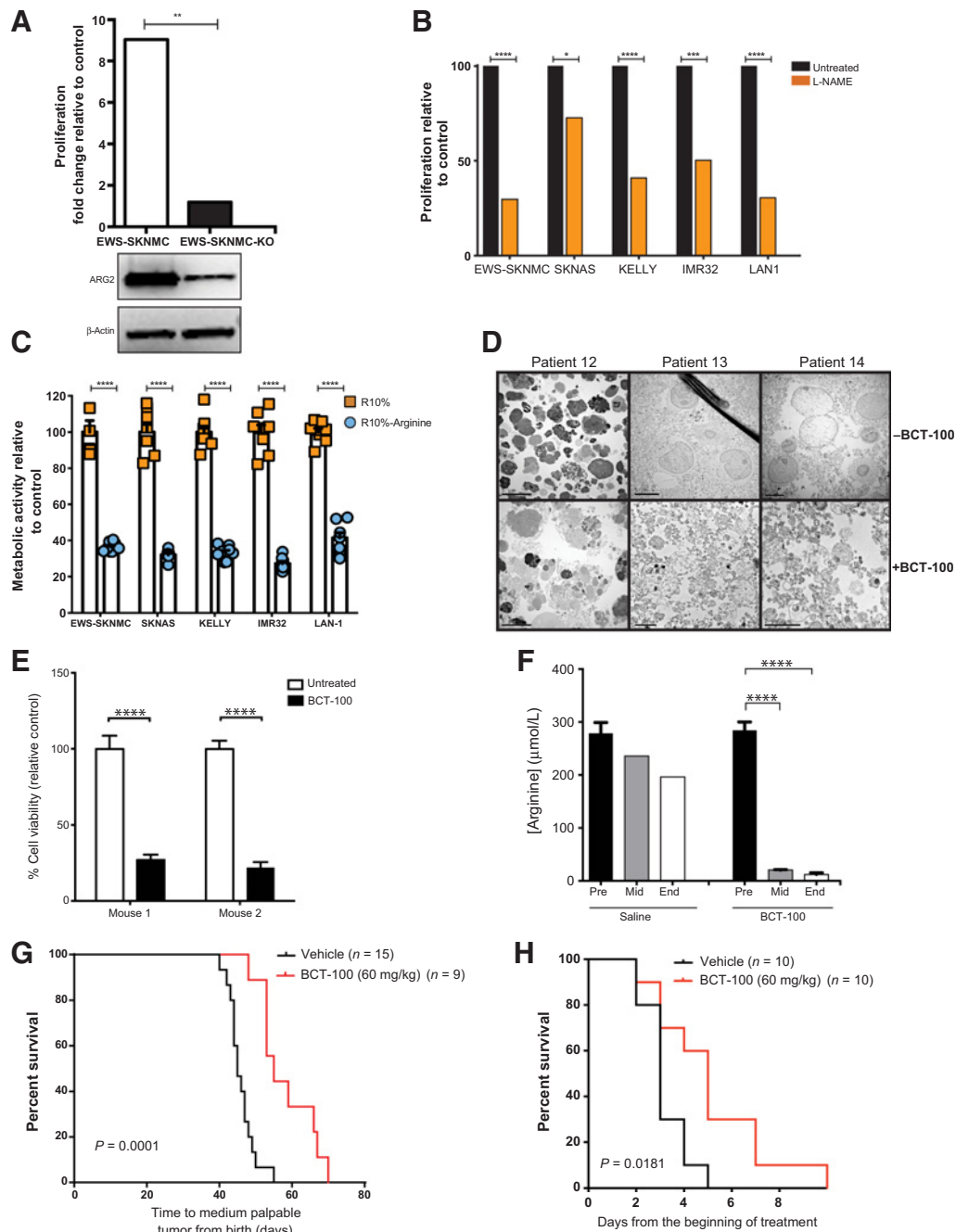
**Figure 1.**

Neuroblastoma induces M1 macrophages. **A**, Nonmetric multidimension scaling of stage I (red) and stage IV (blue) tumors at diagnosis shows distinct proteomic profiles for these two stages of tumors. **B**, Proteomic analysis of stage I and IV tumors identifies significantly higher expression of CD14 and CD15 in stage IV tumors. **C**, IHC staining of sections from neuroblastomas showing infiltration of CD14<sup>+</sup> (top) and CD15<sup>+</sup> (bottom) myeloid cells. Representative sections shown of  $n = 27$  tumors, tissue microarray. **D**, Histocores of CD14 and CD15 staining in neuroblastoma tissue microarrays of  $n = 27$  tumors. **E**, CD14<sup>+</sup> monocytes from healthy donors cocultured with sorted GD2<sup>+</sup> tumor cells from patients upregulate CD68 expression (top). Minimal CD206 upregulation was seen. Representative flow cytometry shown ( $n = 5$ ). **F**, CD14<sup>+</sup> monocytes from healthy donors cocultured with neuroblastoma have decreased arginase activity, as assessed by conversion of ornithine to urea in a colorimetric assay ( $n = 3$ ). **G**, IHC staining of sections from neuroblastomas showing infiltration of CD68<sup>+</sup> macrophages. Representative sections shown of  $n = 27$  tumors, tissue microarray. \*,  $P < 0.05$ ; \*\*,  $P < 0.01$ .

Fultang et al.

**Figure 2.**

Tumor-induced macrophage cells release IL1 $\beta$  and TNF $\alpha$  through p-AKT signaling. ELISA of supernatants following coculture of healthy donor monocytes with neuroblastoma cell lines, showing increased IL1 $\beta$  (A) and TNF $\alpha$  (B);  $n = 7$ . C, Coculture of monocytes from healthy donors with tumor cell lines for 48 hours leads to upregulation of IL1 $\beta$  and TNF $\alpha$  expression, compared with those cultured in RPMI10% media. Flow cytometry staining shown, gated on CD14<sup>+</sup> cells. Representative staining from three independent experiments. D, IHC staining of sections from neuroblastomas showing infiltration of CD33<sup>+</sup>IL1 $\beta$ <sup>+</sup> and CD33<sup>+</sup>TNF $\alpha$ <sup>+</sup> macrophages. Representative sections from  $n = 27$  tissue microarray are shown. E, CD14<sup>+</sup> myeloid cells from healthy donors were sorted following coculture with neuroblastoma cell lines. Coculture leads to increased expression of p-AKT, as shown by Western blotting ( $n = 3$ ). Addition of AKT inhibitor MK2206 to cocultures of CD14<sup>+</sup> cells and neuroblastoma cell lines leads to inhibition of IL1 $\beta$  (F) and TNF $\alpha$  (G) release ( $n = 3$ ) protein expression. \*,  $P < 0.05$ ; \*\*,  $P < 0.01$ ; \*\*\*\*,  $P < 0.0001$ .

**Figure 3.**

Neuroblastoma proliferation is dependent on arginine metabolism. **A**, shRNA knockout of *ARG2* in SKNMC (high baseline *ARG2* expression) decreases cell proliferation. Fold change in cell numbers after 72 hours compared with baseline. Experiment performed in duplicate. Corresponding Western blots for *ARG2* in wild-type and knockdown cell lines are shown below, with actin as a loading control. **B**, Proliferation of tumor cell lines is inhibited by CAT1 inhibition with L-NAME, measured by  $^3\text{H}$ -thymidine incorporation after 72 hours. **C**, Cell lines were cultured with RPMI $^{+}$  10%FBS (R10%) or arginine-free RPMI $^{+}$  10%FBS (R10% arginine). Metabolic activity was measured by MTT after 72 hours.  $n = 7$  replicates. **D**, Sorted  $\text{GD2}^{+}$  neuroblastoma cells from patients were treated with BCT-100 (600 ng/mL). Analysis of cell death was performed by transmission electron microscopy (representative micrographs of 2 of 6 patients shown). Top, untreated cells. Bottom, posttreatment with 600 ng/mL BCT-100. Features consistent with organelle enlargement, cell membrane permeabilization, and cellular fragmentation with 600 ng/mL BCT-100. Experiments were performed on three separate occasions. **E**, Sorted  $\text{GD2}^{+}$  cells from TH-MYCN murine neuroblastomas were cultured with BCT-100 (600 ng/mL) for 72 hours. The percentage of viable cells relative to untreated controls was determined by flow cytometry, using propidium iodide staining. BCT-100 leads to a decrease in murine neuroblastoma cell viability *ex vivo*. **F**, Plasma from control (saline) and BCT-100-treated TH-MYCN mice was collected at the start (Pre), 16 days after (Mid), and at tumor endpoint (End). The concentration of arginine was determined by ELISA. BCT-100 maintains a significant reduction in the plasma arginine concentration *in vivo*.  $n = 6$ . **G**, TH-MYCN mice were treated with BCT-100 (60 mg/kg) twice weekly intraperitoneally (i.p.) from the time of weaning at 3 weeks of age before overt tumor formations (prophylaxis). Kaplan-Meier curves show that the development of tumors is significantly delayed and that survival is increased in BCT-100-treated mice. **H**, TH-MYCN mice were treated with BCT-100 (60 mg/kg) twice weekly i.p. once 5-mm tumors were palpable (treatment). Kaplan-Meier curves show significant prolongation of survival in BCT-100-treated mice. \*,  $P < 0.05$ ; \*\*,  $P < 0.01$ ; \*\*\*,  $P < 0.001$ ; \*\*\*\*,  $P < 0.0001$ .

neuroblastoma cells with low basal expression of ARG2 (SKNAS and IMR32) with IL1 $\beta$  and TNF $\alpha$ , either alone or in combination, resulted in upregulated ARG2 expression (Fig. 4A and B). Sorted human GD2<sup>+</sup> neuroblastoma cells similarly upregulated ARG2 in response to cytokines (Fig. 4C). Consistent with this finding, supernatants from tumor-induced macrophages upregulated ARG2 in neuroblastoma cells (Fig. 4D; Supplementary Fig. S5D). To investigate whether the M1 macrophages would therefore enhance neuroblastoma cell proliferation via ARG2, we cultured neuroblastoma cells with induced macrophage supernatants. Supernatants led to increased cell proliferation in neuroblastoma cells (Fig. 4E, red) compared with the untreated cells (Fig. 4E, black). The phenotype was partially reversed by the addition of IL1 $\beta$  and TNF $\alpha$  neutralizing antibodies (Fig. 4E, green; Supplementary Fig. S5E).

Neuroblastoma is a pathologic derivative of trunk-level neural crest cells, which normally develop into diverse populations including catecholamine-secreting cells of the adrenal medulla, sympathetic, parasympathetic and sensory neurons, and multipotent Schwann cell precursors (22, 23). We hypothesized that a microenvironment containing similar factors to postnatal inflammation may contribute to tumor initiation by upregulating ARG2 in these embryological cells. Analogous to neuroblastoma, treating cultures of normal human embryonic ganglion precursors with IL1 $\beta$  and TNF $\alpha$  led to a significant upregulation of ARG2 protein expression (Fig. 4F), demonstrating the inherent responsiveness of neural crest progenitors to these signals before oncogenic transformation.

We determined that neuroblastoma expresses the receptors for IL1 $\beta$  and TNF $\alpha$  (Fig. 5A). The IL1R1 and TNFR1 receptors can induce a signaling cascade that both converge on a common final effector pathway through ERK1/2 and p38 activation, and ribosomal protein S6 kinase A5 (MSK1) activation (Fig. 5B; refs. 24–26). Treatment of neuroblastoma cells with IL1 $\beta$  and TNF $\alpha$  leads to NF $\kappa$ B phosphorylation by 0.5 hours and subsequent phosphorylation of ERK1/2 from 1 hour onward (Fig. 5C). Simultaneously, the cytokines also induced p38 phosphorylation at 0.5 hours (Fig. 5C). PD98059 binds inactive ERK and prevents phosphorylation and activation by upstream mediators, whereas SB20308 inhibits p38 catalytic activity but does not affect phosphorylation. The resulting inhibition of p38 or ERK1/2 signaling leads to subsequent downregulation of ARG2 expression in SKNAS neuroblastoma cells (Fig. 5D). Blockade of either p38 or ERK1/2 in isolation is insufficient to prevent ARG2 upregulation by cytokines due to compensation by the other side of the pathway (Fig. 7B; Supplementary Fig. S5F). MSK1 is at crossroads of the common downstream cascade and can be autoregulated by kinases including ERK1/2 and p38. SB747651A blockade of MSK1 activity, which is phosphorylated from 0.5 hours onward (Fig. 5C), similarly prevented cytokine-induced ARG2 upregulation (Fig. 5E).

#### The 1 $\beta$ - and TNF $\alpha$ -enriched intratumoral microenvironment is associated with high-stage disease

We previously showed that ARG2 expression is highest in stage IV tumors and is associated with a worse overall survival (9). Cytokines may be functional either within the tumor microenvironment or released into the blood to induce systemic effects. Analysis of blood from 25 patients with neuroblastoma at diagnosis revealed that the majority of patients did not have significantly increased TNF $\alpha$  and IFN $\gamma$  compared with healthy controls,

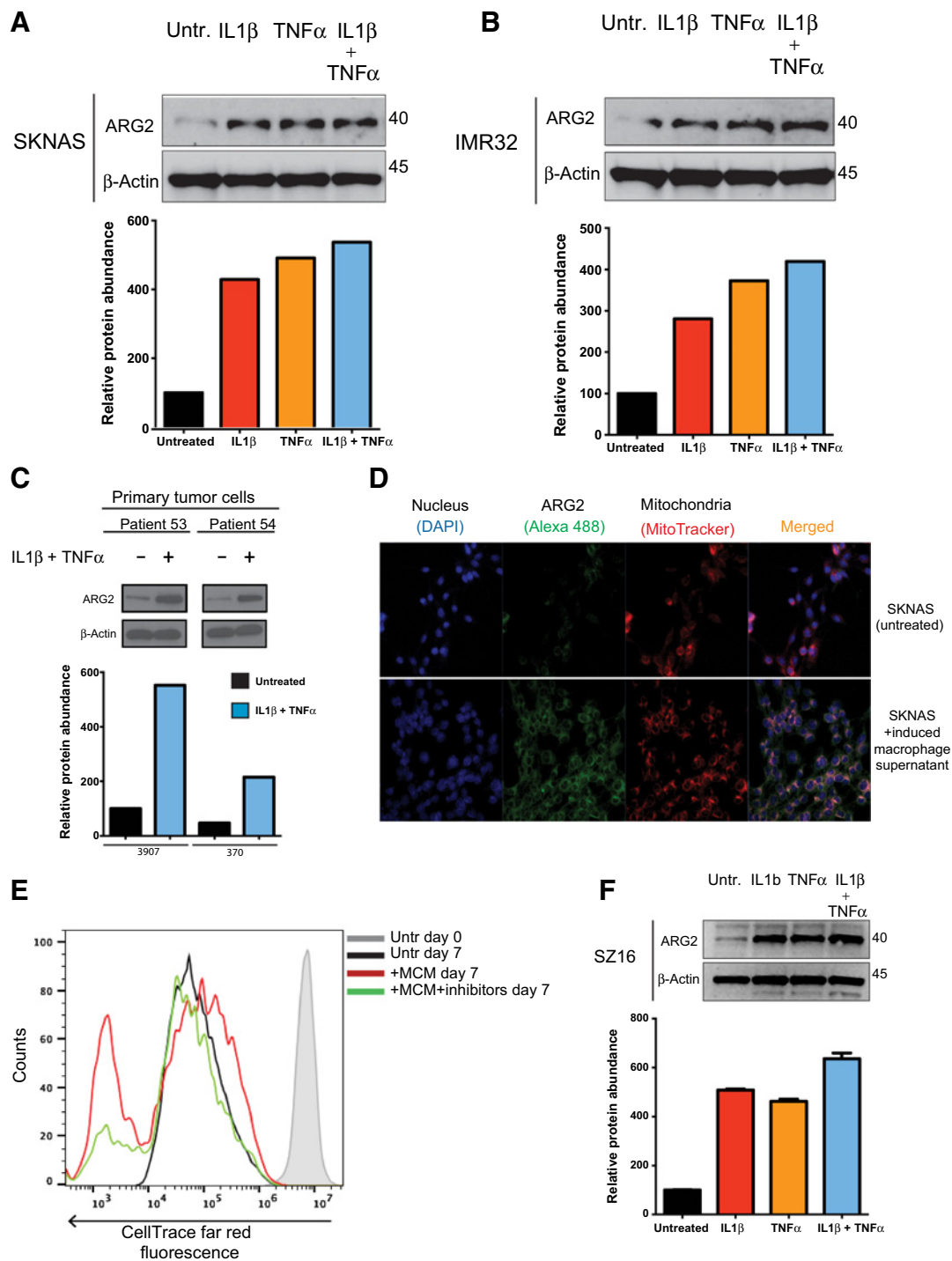
although in 9 cases circulating levels of IL1 $\beta$  and IL6 were significantly higher ( $P = 0.042$ ; Fig. 6A).

We hypothesized that the intratumoral cytokines driving arginine metabolism in neuroblastoma would promote high-stage human neuroblastoma development. To investigate this, we further analyzed the proteomic profile inside 23 human neuroblastoma tumors. Heat map representation of protein signals reveal that stage I and IV tumors show distinct molecular proteomic subgroups, with 7 stage IV tumors (P21–27) forming a distinct group, whereas 3 others (P10, P15, and P16) had proteomes more similar to stage I tumors (Fig. 6B). Consistent with our *in vitro* findings, characterization of the stage IV tumors identified significantly higher levels of the M1 macrophage-derived cytokines IL1 $\beta$  and TNF $\alpha$  than stage I tumors (Fig. 6C). In contrast, stage I tumors had increased expression of the M2-related cytokines TGF $\beta$ , IL10, and IL4 (Fig. 6D). No significant differences in IL6 and IL13 expression were identified. Consistent with this, analysis of the expression profile of 88 neuroblastomas (GEOID: GSE16476) revealed high expression of IL1 $\beta$  or TNF $\alpha$  within tumors is associated with a significantly worse overall survival for patients with neuroblastoma ( $P = 0.012$  and  $P = 0.027$ , respectively, Fig. 7A and B).

## Discussion

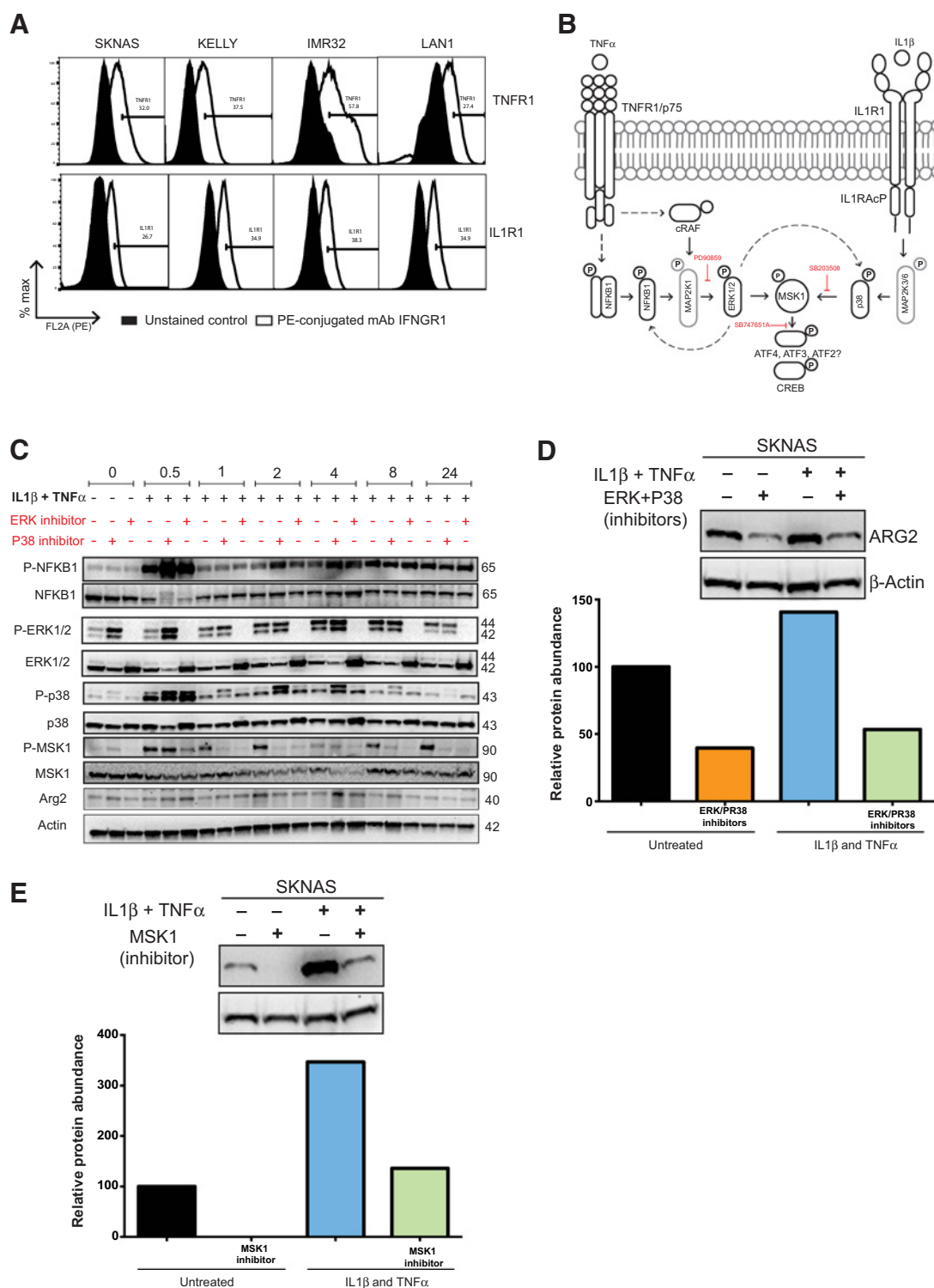
Although it is well established that amino acid metabolism can regulate anticancer immunity, the capacity of the immune system to regulate cancer amino acid metabolism has rarely been characterized. In this study, we identify a key reciprocal regulation between tumor cell arginine metabolism and intratumoral macrophages in neuroblastoma. The regulators of ARG2 expression in cancer are poorly understood despite abundant data on its cytoplasmic counterpart ARG1. ARG2 can be upregulated by hypoxia in osteosarcoma cells and nonmalignant cells, while in pancreatic ductal adenocarcinoma models, obesity correlated with increased ARG2 levels and enhanced tumor growth (27–30). Studies of cytokine regulation of arginase 2 are limited to nonmalignant cells, with reports that Th1 or Th2 cytokines have no effects on murine myeloid cells or can modulate ARG2 expression in murine neural stem cells (31). In humans, IL10 may regulate ARG2 in combination with isoproterenol in macrophages (32).

We and others have previously reported the ability of neuroblastoma to modulate circulating monocytes into an immunosuppressive phenotype on T cells and NKT cells (33). Here we demonstrate that the tumor cells also polarize intratumoral monocytes to M1 macrophages, which express and release IL1 $\beta$  and TNF $\alpha$  after AKT signal transduction. AKT inhibitors, such as Perifosine, have recently undergone early-phase clinical trial development, including evaluation in refractory neuroblastoma, with initial results suggesting that targeting this pathway could prolong progression-free survival (34). We show that tumor-polarized macrophages act back to regulate cancer cell arginine metabolism through IL1 $\beta$  and TNF $\alpha$  and drive tumor cell proliferation. Recently, murine macrophages were shown to increase neuroblastoma proliferation in association with STAT3 phosphorylation, although the factor responsible was not identified (35). We demonstrate that ARG2 expression is under the control of both p38 and ERK1/2 in human neuroblastoma cells, which lie downstream of the receptors for IL1 $\beta$  and TNF $\alpha$  (IL1R1 and TNFR1, respectively). The role of these cytokine pathways in

**Figure 4.**

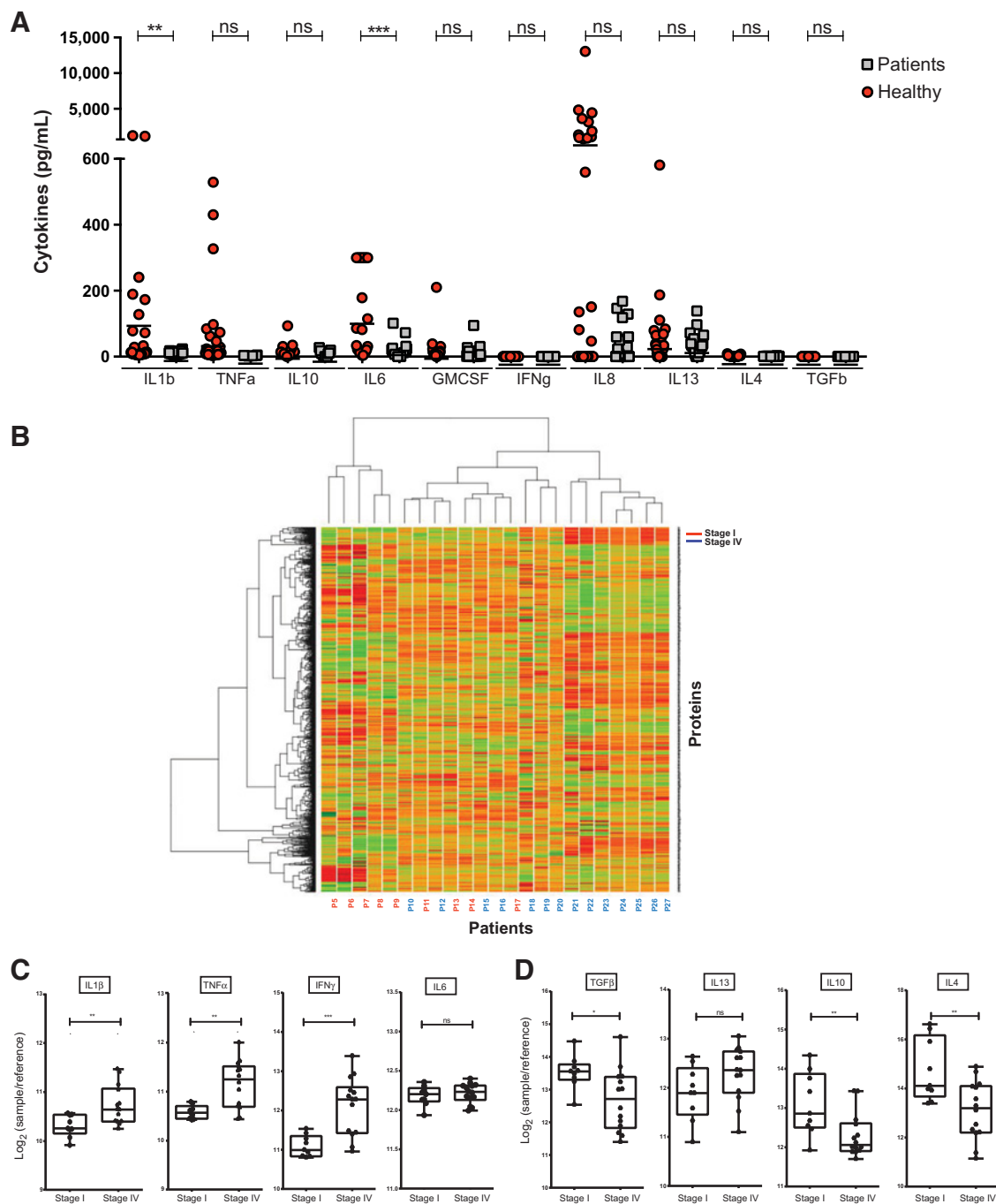
IL1 $\beta$  and TNF $\alpha$  upregulate arginase 2 expression and tumor cell proliferation. Treatment of neuroblastoma cells SKNAS (**A**) and IMR32 (**B**) with recombinant cytokines alone or in combination leads to upregulation of ARG2, measured by Western blot. Actin is shown as a loading control. Corresponding densitometry of ARG2 relative to actin shown. Representative of  $n = 6$  replicates. **C**, Treatment of sorted GD2<sup>+</sup> primary neuroblastoma cells (patients 53 and 54) with cytokines leads to upregulation of ARG2, measured by Western blot. Actin is shown as a loading control. Corresponding densitometry of ARG2 relative to actin shown. **D**, Representative confocal microscopy of neuroblastoma cell line SKNAS shows expression of arginase 2 is increased following culture with the supernatants of neuroblastoma-induced macrophages. DAPI, blue; ARG2, green; MitoTracker, red ( $n = 3$ ). **E**, Neuroblastoma cell proliferation is enhanced in the presence of neuroblastoma-induced macrophage-conditioned supernatants (MCM). The addition of anti-TNF $\alpha$  and IL1 $\beta$  antibodies (inhibitors) reversed the proliferative effects of MCM. Cell proliferation of neuroblastoma is shown by dilution of Cell Trace reagent, measured by flow cytometry. **F**, Treatment of embryonic dorsal root ganglion stem cell line SZ16 with recombinant cytokines alone or in combination leads to upregulation of ARG2, as measured by Western blot. Actin is shown as a loading control. Corresponding densitometry of ARG2 relative to actin shown. Representative of  $n = 3$  replicates.

Fultang et al.



**Figure 5.**

IL1 $\beta$  and TNF $\alpha$  drive arginase 2 expression in a p38/ERK-dependent manner. **A**, Neuroblastoma cell lines express the IL1 $\beta$  and TNF $\alpha$  receptors on the cell surface as assessed by flow cytometry ( $n = 3$ ). **B**, Schematic showing the signaling pathway for IL1 $\beta$  and TNF $\alpha$  cytokines, via ERK1/2, p38, and MSK1. **C**, Time course (hours) in which IL1 $\beta$  and TNF $\alpha$  lead to increased p-NF $\kappa$ B (0.5 hours), p-ERK1/2 (from 1 hour onward), p-p38 (0.5 hours), and p-MSK1 (0.5 hours onward). ERK1/2, p38, and MSK1 activity are inhibited by PD90859, SB203508, and SB747651A, respectively. Western blot shown. Representative of  $n = 3$  replicates. **D**, Treatment of SKNAS neuroblastoma cells with recombinant cytokines leads to upregulation of ARG2, which is inhibited by ERK1/2 and p38 inhibition. Western blot shown with actin as a loading control. Corresponding densitometry of ARG2 relative to actin is shown,  $N = 3$  replicates. **E**, Treatment of SKNAS neuroblastoma cells with recombinant cytokines leads to upregulation of ARG2, which is inhibited by MSK1 inhibition. Western blot is shown, with actin as a loading control. Corresponding densitometry of ARG2 relative to actin shown,  $n = 3$  replicates.

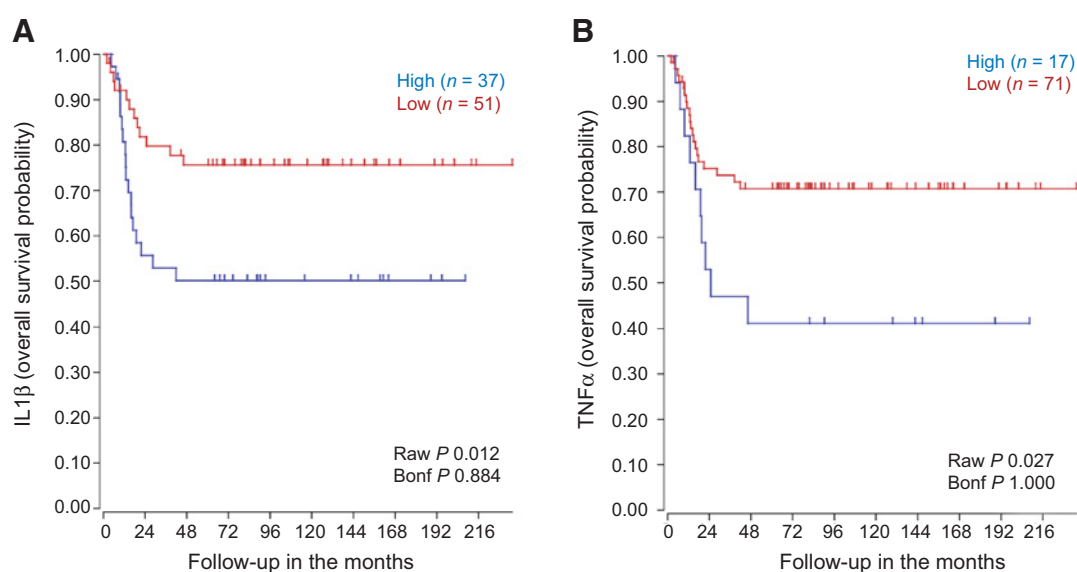
**Figure 6.**

The stage IV neuroblastoma intratumoral microenvironment is enriched in IL1 $\beta$  and TNF $\alpha$ . **A**, ELISA quantification of cytokine titers in neuroblastoma patient plasma ( $n = 26$ ) at diagnosis identifies no significant differences in circulating levels of TNF $\alpha$  and IFN $\gamma$ . Circulating IL1 $\beta$  concentrations were significantly higher in some patients at diagnosis. **B**, Heat map of stage I (red) and stage IV (blue) tumors at diagnosis shows distinct proteomic profiles for these two stages of tumors. **C**, Proteomic analysis of stage I and IV tumors at diagnosis identifies significantly higher expression of the IL1 $\beta$ , TNF $\alpha$ , as well as IFN $\gamma$  in stage IV tumors. **D**, Stage I tumors express significantly higher Th2 cytokines TGF $\beta$ , IL10, and IL4 by proteomic analysis. \*,  $P < 0.05$ ; \*\*,  $P < 0.01$ ; \*\*\*,  $P < 0.001$ ; ns, nonsignificant.

cancer cell expression of ARG2 has not previously been reported. Some redundancy in the signaling cascade is evident, such that inhibition of both receptor pathways, or of their common effect on MSK1, is required to inhibit enzyme expression.

We showed that the stage IV intratumoral microenvironment is enriched in the expression of IL1 $\beta$  and TNF $\alpha$  while the converse is true for stage I tumors. To date, the role of IL1 $\beta$  and TNF $\alpha$  in neuroblastoma has primarily centered around the effects of these

Fultang et al.

**Figure 7.**

High IL1 $\beta$  or TNF $\alpha$  expression in tumors correlates with a worse overall survival for patients Kaplan-Meier curves of  $n = 88$  patients with neuroblastoma at diagnosis identifying high IL1 $\beta$  (**A**) or TNF $\alpha$  (**B**) expression in tumors is associated with a worse overall survival. All data are analyzed in accordance with the public Versteeg database "R2: microarray analysis and visualization platform" (<https://hgserver1.amc.nl/cgi-bin/r2/main.cgi>).

cytokines on neuroblastoma cell lines used as models of neurodegenerative disease, such as Alzheimer disease. In terms of its effects on the malignant phenotype, recombinant TNF $\alpha$  has been shown to be a growth factor for neuroblastoma cell lines, although the mechanism of action was unknown (36). A minor subset of neuroblastoma cells within tumors may themselves express TNF $\alpha$  intracellularly or on the cell membrane, but they do not release the cytokine into the microenvironment (33). For IL1 $\beta$ , little is known in the context of neuroblastoma, although it is reported to drive cyclo-oxygenase (COX-2) expression in neuroblastoma Alzheimer disease cell line models (37). Importantly, we identified that levels of IL1 $\beta$  and TNF $\alpha$  proteins in the plasma are not significantly greater than in healthy donors, indicating that it is the intratumoral interactions that are key.

Clinically, it is clear that stage I and IV neuroblastomas are distinct at the levels of tumor dissemination, responses to chemotherapy, and patient outcome. Intercellular signaling within tumors remains difficult to characterize, although much has been learned from transcriptomic and epigenetic profiling of these tumors (38, 39). The functional interaction of proteins within the cellular ecosystem must be contributing to variation in tumor aggressiveness, although analysis of multiple proteins inside tumors is challenging. To our knowledge, this study is also the first proteomic characterization of human neuroblastomas at diagnosis, and the findings suggest that array-based proteomic profiling can lead to new insights into tumor immunobiology. It has been hypothesized that an immune-stimulatory event, such as infection in early childhood, could contribute to the development of childhood cancers either through a normal or aberrant response. Indeed, a "delayed infection" hypothesis had been suggested for childhood acute lymphoblastic leukemia (40). Although specific infections like Epstein-Barr virus are directly linked to malignant transformation of cells in Hodgkin lymphoma or nasopharyngeal carcinoma, in the majority of pediatric malignancies, no evidence of clearly defined cause and effect has

been found (41, 42). It is possible that an isolated proinflammatory response within a tissue microenvironment could potentially lead to a cytokine profile that drives metabolism in malignant or premalignant cells, giving them a survival advantage, allowing development into a frank malignancy. The inflammation could be secondary to very specific infectious agents or an abnormal, pathologic response due to immune defects.

Neural crest cells are highly multipotent stem cells in the embryo, which give rise to diverse cell types such as melanocytes, odontoblasts, peripheral neurons, and support cells, including those of the dorsal root, sympathetic and parasympathetic ganglia, and specific endocrine cells in the thyroid and parathyroid glands and the adrenal medulla (22). We found that neural crest-derived primary cells are enriched in ARG2 protein, relative to ARG1. The role of ARG2 in embryological processes is not well understood. Neonatal CD71<sup>+</sup> erythroid cells express ARG2, which may affect the response to commensal bacteria in the developing baby, whereas dendritic cells in the developing fetus also express ARG2 to modulate immune responses *in utero* (43, 44). That the expression of ARG2 in untransformed neural crest-derived stem cells can be upregulated by immune cytokines IL1 $\beta$  and TNF $\alpha$  points to the potential for metabolic changes to occur during malignant transformation or expansion. We have previously shown that AML blasts have similarly upregulated ARG2 in comparison with their nonmalignant hematopoietic counterparts (10). Indeed, knockdown of ARG2 significantly reduces the ability of both types of tumor cells to proliferate, suggesting this enzyme provides an advantage to cancer growth and dissemination.

Although arginine metabolism under cytokine control can drive neuroblastoma proliferation, this axis also provides a potential therapeutic target. Targeting tumor-associated myeloid cells has received significant attention to date. Although depletions of myeloid cells can be achieved *in vivo* using anti-GR1 or anti-CR2 antibodies, the effects are very short-lived in mice and no human equivalent exists for clinical translation. One approach to target

the feedback loop we have described is to inhibit IL1 $\beta$  and TNF $\alpha$  cytokine activity. Anti-TNF $\alpha$  therapy was the paradigm for anticytokine therapies with the development of anti-TNF $\alpha$  antibody (infliximab) and a decoy anti-TNF-A receptor (etanercept). Although these antibodies have demonstrated remarkable activity in autoimmune conditions, they have undergone only limited study in the setting of cancer therapy. Infliximab has been used as a single agent in patients with advanced cancer, with some patients experiencing disease stabilization (45). The drug has also been trialed to treat renal cell carcinoma, and although improvements in immune profiles were noted, there were also significant increases in adverse events (46, 47). Similar antibodies against IL1 $\beta$  (canakinumab) and its receptor IL1R1 (anakinra) also exist. Although canakinumab has not been formally tested in patients with an existing cancer, administration of this drug has been shown to significantly reduce incidences of lung cancer and its mortality in patients with atherosclerosis (48). Future combination clinical trials of these agents could represent a novel and potential approach in children with neuroblastoma.

It is now possible to successfully target cancer arginine metabolism through therapeutic arginine depletion with BCT-100, a PEGylated recombinant arginase that induces sustained arginine depletion for months in human trials (49, 50). The drug has completed phase I/II trials in adult malignancies with an excellent safety profile (21). In this study, we demonstrated that BCT-100 leads not only to a decrease in neuroblastoma proliferation with accompanying cell death *in vitro*, but also to delayed progression and prolonged survival in neuroblastoma-bearing mice. These findings support the testing of BCT-100 in an international phase I/II clinical trial (PARC, NCT03455140) in children with relapsed/refractory malignancies, including neuroblastoma. The targeting of both immune and metabolic drivers of tumorigenesis as presented in this study is rational and clinically achievable, and could be a new paradigm in the treatment of neuroblastoma.

### Disclosure of Potential Conflicts of Interest

No potential conflicts of interest were disclosed.

### References

1. Angelin A, Gil-de-Gomez L, Dahiya S, Jiao J, Guo L, Levine MH, et al. Foxp3 Reprograms T cell metabolism to function in low-glucose, high-lactate environments. *Cell Metab* 2017;25:1282–93.e7.
2. Calcinotto A, Filipazzi P, Griotti M, Iero M, De Milito A, Ricupito A, et al. Modulation of microenvironment acidity reverses anergy in human and murine tumor-infiltrating T lymphocytes. *Cancer Res* 2012;72:2746–56.
3. Ho PC, Bihuniak JD, Macintyre AN, Staron M, Liu X, Amezcua R, et al. Phosphoenolpyruvate is a metabolic checkpoint of anti-tumor T cell responses. *Cell* 2015;162:1217–28.
4. Dietl K, Renner K, Dettmer K, Timischl B, Eberhart K, Dorn C, et al. Lactic acid and acidification inhibit TNF secretion and glycolysis of human monocytes. *J Immunol* 2010;184:1200–9.
5. Wei G, Twomey D, Lamb J, Schlis K, Agarwal J, Stam RW, et al. Gene expression-based chemical genomics identifies rapamycin as a modulator of MCL1 and glucocorticoid resistance. *Cancer Cell* 2006;10:331–42.
6. Fultang L, Vardon A, De Santo C, Mussai F. Molecular basis and current strategies of therapeutic arginine depletion for cancer. *Int J Cancer* 2016;139:501–9.
7. Morris SM Jr. Arginine Metabolism Revisited. *J Nutr* 2016;146:2579S–86S.
8. De Santo C, Arscott R, Booth S, Karydis I, Jones M, Asher R, et al. Invariant NKT cells modulate the suppressive activity of IL-10-secreting neutrophils differentiated with serum amyloid A. *Nat Immunol* 2010;11:1039–46.
9. Mussai F, Egan S, Hunter S, Webber H, Fisher J, Wheat R, et al. Neuroblastoma Arginase activity creates an immunosuppressive microenviron-

### Authors' Contributions

**Conception and design:** L. Fultang, L. Gneo, P.N. Cheng, M.D. Norris, J. Murray, C. De Santo, F. Mussai

**Development of methodology:** L. Fultang, L.D. Gamble, A.M. Berry, S.A. Egan, S. Brownhill, L. Chesler, S.A. Burchill, M. Haber, C. De Santo, F. Mussai

**Acquisition of data (provided animals, acquired and managed patients, provided facilities, etc.):** L. Fultang, L.D. Gamble, L. Gneo, A.M. Berry, F. De Bie, O. Yogev, S. Brownhill, A. Vardon, C.M. McConville, H.C. Etchevers, J. Murray, D.S. Ziegler, L. Chesler, R. Schmidt, S.A. Burchill, M. Haber, C. De Santo, F. Mussai

**Analysis and interpretation of data (e.g., statistical analysis, biostatistics, computational analysis):** L. Fultang, L. Gneo, S.A. Egan, P.N. Cheng, J. Murray, L. Chesler, R. Schmidt, S.A. Burchill, C. De Santo, F. Mussai

**Writing, review, and/or revision of the manuscript:** L. Fultang, L. Gneo, A.M. Berry, S.A. Egan, O. Yogev, S. Brownhill, C.M. McConville, M.D. Norris, H.C. Etchevers, J. Murray, D.S. Ziegler, L. Chesler, R. Schmidt, S.A. Burchill, C. De Santo, F. Mussai

**Administrative, technical, or material support (i.e., reporting or organizing data, constructing databases):** L. Fultang, F. De Bie, G.L. Eden, S. Booth, A. Vardon, P.N. Cheng, S.A. Burchill, C. De Santo

**Study supervision:** M.D. Norris, D.S. Ziegler, S.A. Burchill, C. De Santo, F. Mussai

### Acknowledgments

The authors thank the patients and parents who contributed samples to the study as well as Jane Cooper and Cay Shakespeare for obtaining consent and collection of patient samples. We also thank Paul Stanley and Theresa Morris for technical assistance with electron microscopy. This work was supported by Cancer Research UK, Niayah's Fund, Neuroblastoma UK, Children with Cancer, Treating Children with Cancer, Children's Cancer and Leukaemia Group, the Association Française contre les Myopathies, grants from the National Health and Medical Research Council Australia, Cancer Institute, AKO Foundation, and the alumni and donors to the University of Birmingham.

The costs of publication of this article were defrayed in part by the payment of page charges. This article must therefore be hereby marked *advertisement* in accordance with 18 U.S.C. Section 1734 solely to indicate this fact.

Received July 13, 2018; revised October 19, 2018; accepted December 5, 2018; published first December 13, 2018.

- ment that impairs autologous and engineered immunity. *Cancer Res* 2015;75:3043–53.
10. Mussai F, De Santo C, Abu-Dayyeh I, Booth S, Quek L, McEwen-Smith RM, et al. Acute myeloid leukemia creates an arginase-dependent immunosuppressive microenvironment. *Blood* 2013;122:749–58.
11. Weiss W, Aldape K, Mohapatra G, Feuerstein B, Bishop J. Targeted expression of MYCN causes neuroblastoma in transgenic mice. *EMBO J* 1997;16:2985–95.
12. Haraguchi S, Nakagawara A. A simple PCR method for rapid genotype analysis of the TH-MYCN transgenic mouse. *PLoS One* 2009;4:e6902.
13. Thomas S, Thomas M, Wincker P, Babarit C, Xu P, Speer MC, et al. Human neural crest cells display molecular and phenotypic hallmarks of stem cells. *Hum Mol Genet* 2008;17:3411–25.
14. de Pontual L, Zaghloul NA, Thomas S, Davis EE, McCaughey DM, Dollfus H, et al. Epistasis between RET and BBS mutations modulates enteric innervation and causes syndromic Hirschsprung disease. *PNAS* 2009;106:13921–6.
15. Boeva V, Louis-Brennetot C, Peltier A, Durand S, Pierre-Eugène C, Raynal V, et al. Heterogeneity of neuroblastoma cell identity defined by transcriptional circuitries. *Nat Genet* 2017;49:1408.
16. Schroder C, Srinivasan H, Sill M, Linseisen J, Fellenberg K, Becker N, et al. Plasma protein analysis of patients with different B-cell lymphomas using high-content antibody microarrays. *Proteomics Clin Appl* 2013;7:802–12.

Fultang et al.

17. Sill M, Schroder C, Hoheisel JD, Benner A, Zucknick M. Assessment and optimisation of normalisation methods for dual-colour antibody microarrays. *BMC Bioinformatics* 2010;11:556.
18. Ruiz-Babot G, Balyura M, Hadjidemetriou I, Ajodha SJ, Taylor DR, Ghattaore L, et al. Modeling congenital adrenal hyperplasia and testing interventions for adrenal insufficiency using donor-specific reprogrammed cells. *Cell Rep* 2018;22:1236–49.
19. Engblom C, Pfrschke C, Pittet MJ. The role of myeloid cells in cancer therapies. *Nat Rev Cancer* 2016;16:447–62.
20. Xie S, Chen M, Yan B, He X, Chen X, Li D. Identification of a role for the PI3K/AKT/mTOR signaling pathway in innate immune cells. *PLoS One* 2014;9:e94496.
21. Yau T, Cheng PN, Chan P, Chen L, Yuen J, Pang R, et al. Preliminary efficacy, safety, pharmacokinetics, pharmacodynamics and quality of life study of pegylated recombinant human arginase 1 in patients with advanced hepatocellular carcinoma. *Invest New Drugs* 2015;33:496–504.
22. Le Douarin N, Kalcheim C. *The neural crest*. 2nd ed. Cambridge, UK; New York, NY: Cambridge University Press; 1999. xxiii, 445 pp.
23. Espinosa-Medina I, Outin E, Picard CA, Chettouh Z, Dymecki S, Consalez GG, et al. Neurodevelopment. Parasympathetic ganglia derive from Schwann cell precursors. *Science* 2014;345:87–90.
24. Turner MD, Nedjai B, Hurst T, Pennington DJ. Cytokines and chemokines: At the crossroads of cell signalling and inflammatory disease. *Biochim Biophys Acta* 2014;1843:2563–82.
25. Campbell J, Ciesielski CJ, Hunt AE, Horwood NJ, Beech JT, Hayes LA, et al. A Novel Mechanism for TNF- Regulation by p38 MAPK: Involvement of NF- B with Implications for Therapy in Rheumatoid Arthritis. *J Immunol* 2004;173:6928–37.
26. Qin J, Jiang Z, Qian Y, Casanova JL, Li X. IRAK4 kinase activity is redundant for interleukin-1 (IL-1) receptor-associated kinase phosphorylation and IL-1 responsiveness. *J Biol Chem* 2004;279:26748–53.
27. Talavera MM, Nuthakki S, Cui H, Jin Y, Liu Y, Nelin LD. Immunostimulated arginase II expression in intestinal epithelial cells reduces nitric oxide production and apoptosis. *Front Cell Dev Biol* 2017;5:15.
28. Xue J, Nelin LD, Chen B. Hypoxia induces arginase II expression and increases viable human pulmonary artery smooth muscle cell numbers via AMPK $\alpha$ 1 signaling. *Am J Physiol Lung Cell Mol Physiol* 2017;312:L568–L78.
29. Setty BA, Pillay Smiley N, Pool CM, Jin Y, Liu Y, Nelin LD. Hypoxia-induced proliferation of HeLa cells depends on epidermal growth factor receptor-mediated arginase II induction. *Physiol Rep* 2017;5(6). pii: e13175. doi: 10.14814/phy2.13175.
30. Zaytouni T, Tsai PY, Hitchcock DS, DuBois CD, Freinkman E, Lin L, et al. Critical role for arginase 2 in obesity-associated pancreatic cancer. *Nat Commun* 2017;8:242.
31. Munder M, Eichmann K, Moran M, Centeno F, Soler G, Modollel M. Th1/Th2-regulated expression of arginase isoforms in murine macrophages and dendritic cells. *J Immunol* 1999;163:3771–7.
32. Barksdale AR, Bernard AC, Maley ME, Gellin GL, Kearney PA, Boulanger BR, et al. Regulation of arginase expression by T-helper II cytokines and isoproterenol. *Surgery* 2004;135:527–35.
33. Liu D, Song L, Wei J, Courtney AN, Gao X, Marinova E, et al. IL-15 protects NKT cells from inhibition by tumor-associated macrophages and enhances antimetastatic activity. *J Clin Invest* 2012;122:2221–33.
34. Kushner BH, Cheung NV, Modak S, Becher OJ, Basu EM, Roberts SS, et al. A phase I/II trial targeting the Pi3k/Akt pathway using perifosine: Long-term progression-free survival of patients with resistant neuroblastoma. *Int J Cancer* 2017;140:480–4.
35. Hadjidanil M, Muthugounder S, Hung L, Sheard M, Shirinbak S, Chan R, et al. Tumor-associated macrophages promote neuroblastoma via STAT3 phosphorylation and up-regulation of c-MYC. *Oncotarget* 2017;8:91516–29.
36. Goillot E, Combaret V, Ladenstein R, Baubet D, Blay JY, Philip T, et al. Tumor necrosis factor as an autocrine growth factor for neuroblastoma. *Cancer Res* 1992;52:3194–200.
37. Fiebich B, Mueksch B, Boehringer M, Hull M. Interleukin-1beta induces cyclooxygenase-2 and prostaglandin E(2) synthesis in human neuroblastoma cells: involvement of p38 mitogen-activated protein kinase and nuclear factor-kappaB. *J Neurochem* 2000;75:2020–8.
38. Henrich KO, Bender S, Saadati M, Dreidax D, Gartlgruber M, Shao C, et al. Integrative genome-scale analysis identifies epigenetic mechanisms of transcriptional deregulation in unfavorable neuroblastomas. *Cancer Res* 2016;76:5523–37.
39. van Groningen T, Koster J, Valentijn LJ, Zwijnenburg DA, Akogul N, Hasselt NE, et al. Neuroblastoma is composed of two super-enhancer-associated differentiation states. *Nat Genet* 2017;49:1261–6.
40. Greaves M. Infection, immune responses and the aetiology of childhood leukaemia. *Nat Rev Cancer* 2006;6:193–203.
41. Schmidt LS, Kamper-Jorgensen M, Schmiegelow K, Johansen C, Lahteenmaki P, Trager C, et al. Infectious exposure in the first years of life and risk of central nervous system tumours in children: analysis of birth order, childcare attendance and seasonality of birth. *Br J Cancer* 2010;102:1670–5.
42. Hwee J, Tait C, Sung L, Kwong JC, Sutradhar R, Pole JD. A systematic review and meta-analysis of the association between childhood infections and the risk of childhood acute lymphoblastic leukaemia. *Br J Cancer* 2018;118:127–37.
43. Elahi S, Ertel JM, Kinder JM, Jiang TT, Zhang X, Xin L, et al. Immunosuppressive CD71+ erythroid cells compromise neonatal host defence against infection. *Nature* 2013;504:158–62.
44. McGovern N, Shin A, Low G, Low D, Duan K, Yao LJ, et al. Human fetal dendritic cells promote prenatal T-cell immune suppression through arginase-2. *Nature* 2017;546:662–6.
45. Brown ER, Charles KA, Hoare SA, Rye RL, Jodrell DI, Aird RE, et al. A clinical study assessing the tolerability and biological effects of infliximab, a TNF-alpha inhibitor, in patients with advanced cancer. *Ann Oncol* 2008;19:1340–6.
46. Larkin JM, Ferguson TR, Pickering LM, Edmonds K, James MG, Thomas K, et al. A phase I/II trial of sorafenib and infliximab in advanced renal cell carcinoma. *Br J Cancer* 2010;103:1149–53.
47. Harrison ML, Obermueller E, Maisey NR, Hoare S, Edmonds K, Li NF, et al. Tumor necrosis factor alpha as a new target for renal cell carcinoma: two sequential phase II trials of infliximab at standard and high dose. *J Clin Oncol* 2007;25:4542–9.
48. Ridker PM, MacFadyen JG, Thuren T, Everett BM, Libby P, Glynn RJ, et al. Effect of interleukin-1 $\beta$  inhibition with canakinumab on incident lung cancer in patients with atherosclerosis: exploratory results from a randomised, double-blind, placebo-controlled trial. *Lancet North Am Ed* 2017;390:1833–42.
49. Yau T, Cheng PN, Chan P, Chan W, Chen L, Yuen J, et al. A phase 1 dose-escalating study of pegylated recombinant human arginase 1 (Peg-rhArg1) in patients with advanced hepatocellular carcinoma. *Invest New Drugs* 2013;31:99–107.
50. De Santo C, Cheng P, Beggs A, Egan S, Bessudo A, Mussai F. Metabolic therapy with PEG-arginase induces a sustained complete remission in immunotherapy-resistant melanoma. *J Hematol Oncol* 2018;11:68.

# Cancer Research

The Journal of Cancer Research (1916–1930) | The American Journal of Cancer (1931–1940)

## Macrophage-Derived IL1 $\beta$ and TNF $\alpha$ Regulate Arginine Metabolism in Neuroblastoma

Livingstone Fultang, Laura D. Gamble, Luciana Gneo, et al.

*Cancer Res* 2019;79:611-624. Published OnlineFirst December 13, 2018.

**Updated version** Access the most recent version of this article at:  
doi:[10.1158/0008-5472.CAN-18-2139](https://doi.org/10.1158/0008-5472.CAN-18-2139)

**Supplementary Material** Access the most recent supplemental material at:  
<http://cancerres.aacrjournals.org/content/suppl/2018/12/12/0008-5472.CAN-18-2139.DC1>

**Cited articles** This article cites 50 articles, 15 of which you can access for free at:  
<http://cancerres.aacrjournals.org/content/79/3/611.full#ref-list-1>

**E-mail alerts** [Sign up to receive free email-alerts](#) related to this article or journal.

**Reprints and Subscriptions** To order reprints of this article or to subscribe to the journal, contact the AACR Publications Department at [pubs@aacr.org](mailto:pubs@aacr.org).

**Permissions** To request permission to re-use all or part of this article, use this link  
<http://cancerres.aacrjournals.org/content/79/3/611>.  
Click on "Request Permissions" which will take you to the Copyright Clearance Center's (CCC) Rightslink site.